Geosci. Model Dev. Discuss., 7, 2797–2828, 2014
www.geosci-model-dev-discuss.net/7/2797/2014/
doi:10.5194/gmdd-7-2797-2014

Geoscientific Model Development Discussions
Open Access

IL-GLOBO (1.0) – integrated Lagrangian particle model and Eulerian general circulation model GLOBO: development of the vertical diffusion module

D. Rossi[1,2] **and A. Maurizi**[1]

[1]Institute of Climate and Atmospheric Sciences, National Research Council, Bologna, Italy
[2]Department of Biological, Geological and Environmental Sciences, University of Bologna, Bologna, Italy

Received: 6 March 2014 – Accepted: 23 March 2014 – Published: 30 April 2014

Correspondence to: A. Maurizi (a.maurizi@isac.cnr.it)

Published by Copernicus Publications on behalf of the European Geosciences Union.

Abstract

The development and validation of the vertical diffusion module of IL-GLOBO, a Lagrangian transport model coupled online with the Eulerian General Circulation Model GLOBO, is described. The module simulates the effects of turbulence on particle motion by means of a Lagrangian Stochastic Model (LSM) consistent with the turbulent diffusion equation used in GLOBO. The implemented LSM integrates particle trajectories, using the native σ-hybrid coordinates of the Eulerian component, and fulfills the Well Mixed Condition (WMC) in the general case of a variable density profile. The module is validated through a series of 1-D numerical experiments by assessing its accuracy in maintaining an initially well mixed distribution. A dynamical time-step selection algorithm with constraints related to the shape of the diffusion coefficient profile is developed and gives accurate results, even for strongly peaked diffusivity profiles. Finally, the skills of a linear interpolation and a modified Akima spline interpolation method are compared, showing that the former generally introduces deviations from the WMC, due to the inconsistency between the local value of the diffusion coefficient and its derivatives. The Akima interpolation algorithm, for which the model satisfies the WMC rigorously, has a computational cost within 120 % of the linear interpolation algorithm, making it a reasonable option for implementation in the 3-D model.

1 Introduction

Global (or hemispheric) scale transport is recognized as an important issue in air pollution and climate change studies. Pollutants can travel across continents and have an influence even far from their source (see, e.g., Fiore et al., 2011; Yu et al., 2013, among the most recent). Moreover, transport of volcanic emissions (e.g., the recent Eyjafjallajökull eruption) or accidental hazardous releases (like the Fukushima and Chernobyl nuclear accidents) are also important at the global scale.

GMDD
7, 2797–2828, 2014

The natural framework for the description of tracer transport in flows is the Lagrangian approach (see, for example, the seminal works by Taylor, 1921, and Richardson, 1926). In the Lagrangian framework, the tracer transport is described by integrating the kinematic equation of motion for fluid "particles" in a given flow velocity field, provided by, e.g., a meteorological model. The turbulent motion unresolved by Eulerian equations for averaged quantities (in the Reynolds or volume-filtered sense) can be accounted for by including a stochastic component into the kinematic equation.

The stochastic component can be added to the particle position, to give the Lagrangian equivalent of the Eulerian advection–diffusion equation. This kind of model is usually called a Random Displacement Model (RDM) and is suitable for dispersion over long time scales. When the stochastic component is added to the velocity, the model is usually called a Random Flight Model (RFM), which is more suitable for shorter time dispersion. In both cases, the stochastic model formulation has to be consistent with some basic physical requirements (Thomson, 1987, 1995).

Various Lagrangian transport models exist, which can be used at the global scale. Some are designed specifically for the description of atmospheric chemistry (see, e.g., Reithmeier and Sausen, 2002; Wohltmann and Rex, 2009; Pugh et al., 2012), while others focus on the transport of tracers. In the latter class, two of the most widely used models are FLEXPART (Stohl et al., 2005) and HYSPLIT (Draxler and Hess, 1998), which are highly flexible and can be easily used in a variety of situations. Both are compatible with different input types (usually provided by meteorological services like ECMWF), relying on their own parameterization for fields not available from the meteorological model output. Models of this kind are suited for both forward and backward dispersion studies.

An alternative approach is to couple the Eulerian and Lagrangian parts online. On one hand, this makes the Eulerian fields available to the Lagrangian model at each Eulerian time-step, increasing the accuracy for temporal scales shorter than the typical meteorological output interval. On the other hand, it also allows the consistent parameterization of processes in the Eulerian and Lagrangian frameworks (e.g., the vertical

GMDD
7, 2797–2828, 2014

dispersion in the boundary layer). Moreover, where the considered tracer may have an impact on meteorology (e.g., on radiation or cloud micro-physics), online integration provides a natural way to include these effects (Baklanov et al., 2014). Online coupling also ensures the consistency of a mixed Eulerian–Lagrangian analysis of the evolution of atmospheric constituents (e.g., water 0 or pollutants) along a trajectory (see, e.g., Sodemann et al., 2008; Real et al., 2010).

Malguzzi et al. (2011) recently developed a new global numerical weather prediction model, named GLOBO, based on a uniform latitude-longitude grid. The model is an extension to the global scale of the Bologna Limited Area Model (BOLAM) (Buzzi et al., 2004), developed and employed starting from the early 90s. GLOBO is used for daily forecasting at the Institute of Atmospheric Sciences and Climate of the National Research Council of Italy (ISAC-CNR) and is also used to produce monthly forecasts. Online integration with BOLAM family models has already yielded interesting results in the development of the meteorology and composition model BOLCHEM (Mircea et al., 2008). Considering that experience, the GLOBO model constitutes the natural basis for the further development of an Integrated Lagrangian model.

In the following, the development of the vertical diffusion module is presented, focusing in particular on its compliance with basic theoretical requirements (the Well Mixed Condition, see Thomson, 1987, 1995) in connection with different numerical issues. In Sect. 2 the theoretical basis of the model formulation is given, while Sect. 3 describes different aspects of the numerical implementation. Finally, the model verification is presented and discussed in Sect. 4.

2 Lagrangian stochastic model formulation

In application to dispersion in turbulent flows, Lagrangian stochastic models (LSMs), Markovian at order M ($M = 0, 1, \ldots$), are described by a set of stochastic differential equations (SDEs). The equation for the derivative of order M is:

GMDD
7, 2797–2828, 2014

$$dX_i^{(M)} = a_i dt + b_{ij} dW_j, \tag{1}$$

where i and j indicate the components and $X_i^{(k)}$ is the kth order time-derivative of the Lagrangian Cartesian coordinate component $X_i \equiv X_i^{(0)}$. Coefficients a_i and b_{ij} are called drift and Wiener coefficients, respectively. The remaining equations of the set ($1 \le k \le M$) are described by:

$$dX_i^{(k-1)} = X_i^{(k)} dt. \tag{2}$$

The set of equations is equivalent to the Fokker–Planck equation:

$$\frac{\partial p}{\partial t} = -\sum_{k=0}^{M} \frac{\partial}{\partial x_i^{(k)}} (A_i^k p) + \frac{\partial^2}{\partial x_i^{(M)} \partial x_j^{(M)}} (K_{ij} p), \tag{3}$$

where $A_i^k = 1$ for $k < M$ and $A_i^k = a_i$ for $k = M$, x_i is the Eulerian equivalent of X_i and $K_{ij} \equiv b_{ik} b_{kj}/2$ (Thomson, 1987). Equation (3) describes the evolution of the probability density function $p(\mathbf{X}^{(0)}, \ldots, \mathbf{X}^{(M)}, t)$, where $\mathbf{X}^{(k)} = (X_1^{(k)}, X_2^{(k)}, X_3^{(k)})$. For the evolution of $(\mathbf{X}^{(0)}, \ldots, \mathbf{X}^{(M)})$ to be approximated by a Markov process, the time correlation of the variable $\mathbf{X}^{(M+1)}$ has to be much shorter than the characteristic evolution time of $\mathbf{X}^{(M)}$. If the model has to describe the evolution of dispersion at time $t \gg \tau$, where τ is the correlation time of turbulent velocity fluctuations, the process is well captured at order $M = 0$. When shorter times are considered, as in the case of dispersion from a single point source before the Taylor (1921) diffusive regime occurs ($t \le \tau$), order M must be increased to 1. The model of lowest order ($M = 0$, or RDM) is sufficiently accurate to describe transport and mixing of particles at time and space resolution typical of a global model.

The correct formulation of a RDM in a variable density flow was first obtained by Venkatram (1993) and then generalized by Thomson (1995). It is briefly recalled here.

GMDD
7, 2797–2828, 2014

Equation (3) is valid for the pdf p of particle position with the initial condition $p(x,t)|_{t=t_0} = p(x,t_0)$. Since the ensemble average of concentration $\langle c \rangle$ is proportional to p, Eq. (3) can be rewritten as

$$\frac{\partial \langle c \rangle}{\partial t} = -\frac{\partial}{\partial x_i}(a_i \langle c \rangle) + \frac{\partial^2}{\partial x_i \partial x_j}(K_{ij} \langle c \rangle). \tag{4}$$

If $\langle c \rangle \propto \langle \rho \rangle$ at some time t', where $\langle \rho \rangle$ is the ensemble average of air density, then $\forall t > t'$ the two quantities must remain proportional. This condition, called well mixed condition (WMC) after Thomson (1987), implies that $\langle \rho \rangle$ is also a solution of Eq. (4). In order to obtain an expression for the drift coefficient a_i, the most natural choice is to use the continuity equation. In meteorological models it is (Thomson, 1995) written as:

$$\frac{\partial \langle \rho \rangle}{\partial t} = -\frac{\partial}{\partial x_i}\left(\overline{u}_i \langle \rho \rangle\right), \tag{5}$$

where $\overline{u}_i$ is the density weighted velocity, defined as:

$$\overline{u}_i = \frac{\langle u_i \rho \rangle}{\langle \rho \rangle} = \langle u_i \rangle + \frac{\langle u_i' \rho' \rangle}{\langle \rho \rangle}. \tag{6}$$

With this choice, the following expression for the drift term is obtained:

$$a_i = \frac{\partial K_{ij}}{\partial x_j} + \frac{K_{ij}}{\langle \rho \rangle}\frac{\partial \langle \rho \rangle}{\partial x_j} + \overline{u}_i. \tag{7}$$

At the coarse resolution typical of global models, vertical motions can be considered decoupled from the horizontal ones. Therefore, only the vertical coordinate $x_3 \equiv z$ (and $X_3 \equiv Z$ in Lagrangian terms) need to be considered. In this case, the RDM reduces to a single differential stochastic equation

$$\mathrm{d}Z = \left(\overline{w} + \frac{\partial K}{\partial z} + \frac{K}{\langle \rho \rangle}\frac{\partial \langle \rho \rangle}{\partial z}\right)\mathrm{d}t + \sqrt{2K}\mathrm{d}W, \tag{8}$$

where $\overline{w} \equiv \overline{u}_3$ and $K \equiv K_{33}$.

GMDD
7, 2797–2828, 2014

3 Numerical implementation of the vertical diffusion module

In its final form, IL-GLOBO will be a fully online integrated model (or, at least an online-access model, according to Baklanov et al., 2014), where the different components share the same "view" of the atmosphere, i.e., use the same discretization, parameterizations, etc. The development of the vertical diffusion module is based on this principle.

3.1 Vertical coordinate

Within IL-GLOBO, the Lagrangian equations are integrated in the same coordinate system used in the Eulerian Model. This choice maintains the consistency between the Lagrangian and Eulerian components and reduces the interpolation errors and computational cost.

GLOBO uses a hybrid vertical coordinate system in which the terrain-following coordinate σ ($0 < \sigma < 1$) smoothly tends, with height above the ground, to a pressure coordinate P, according to:

$$P = P_0\sigma - (P_0 - P_S)\sigma^{\alpha}, \tag{9}$$

where P_0 is a reference pressure (typically 1000 hPa), P_S is the surface pressure and α is a parameter that gives the classical σ coordinate for $\alpha = 1$ (Phillips, 1957). The parameter α depends on the model orography and, therefore, on resolution. It is limited by the relationship:

$$\alpha \leq \frac{P_0}{P_0 - \min(P_S)}, \tag{10}$$

which is satisfied by the typical setting $\alpha = 2$, used for a wide range of resolutions in GLOBO applications (Malguzzi et al., 2011).

The vertical Lagrangian coordinate is identified by Σ and is connected to the Lagrangian vertical position Z through Eq. (9) and the hydrostatic relationship. In the

GMDD
7, 2797–2828, 2014

meteorological component, z is a diagnostic quantity that can be derived from the geopotential Φ through $z(\sigma) = (\Phi(\sigma) - \Phi_g)g^{-1}$, where Φ_g is the geopotential of the model surface. Since the determination of the different terms in Eq. (8) involves discrete Eulerian fields and their numerical derivatives, the choice to employ σ has also the advantage of making interpolation straightforward and consistent with the Eulerian part.

Because $\sigma(z)$ is not linear (σ is not a Cartesian coordinate system), the stochastic chain rule (see, e.g. Kloeden and Platen, 1992, p. 80) must be used to derive the correct form of Eq. (8) for Σ, giving:

$$d\Sigma = \left[\omega + \frac{K}{\langle\rho\rangle}\frac{\partial\langle\rho\rangle}{\partial\sigma} + \frac{\partial K}{\partial\sigma} + K\frac{\partial^2\sigma}{\partial z^2}\right]dt + \sqrt{2K}dW, \tag{11}$$

where ω is the vertical velocity in the σ coordinate system and z is the Cartesian vertical coordinate. The last term in square brackets stems from the Taylor expansion of order dW^2, which must be included for the correct description at order dt (Gardiner, 1990, p. 63).

3.2 Discretization and interpolation

The GLOBO prognostic variables are computed on a Lorenz (1960) vertical grid: all the quantities are on "integer" levels σ_i, except vertical velocity, turbulent kinetic energy and mixing length and, consequently, diffusion coefficients, located at "semi-integer" levels σ_i^h (see, Fig. 1). In typical applications, the GLOBO vertical grid is regularly spaced in σ (Malguzzi et al., 2011), although it is possible to use a variable grid spacing, as in its limited area version BOLAM (Buzzi et al., 1994).

Being Σ a continuous coordinate, the quantities needed to compute the terms of Eq. (11) must be interpolated from the Eulerian fields given at discrete levels. The computation of first and second order derivatives of Eulerian model quantities is also required in the implementation of the LSM. Interpolation and derivation algorithms can

GMDD
7, 2797–2828, 2014

influence both the accuracy and the computational cost of the Lagrangian model and thus require careful assessment.

Two different methods are tested in the following sections. The first is a simple algorithm, in which the variables and their first- and second-order derivatives, computed on the grid points using a centered 3 point scheme of order $\mathcal{O}(\Delta\sigma^2)$ consistently with the Eulerian component, are interpolated linearly at particle position Σ. The second algorithm is based on the Akima (1970) and Akima (1991) splines. These algorithms reduce the number of oscillations in the interpolating function compared to regular cubic splines. The difference between the two versions is that the linearity of the interpolating function is enforced when 3 (Akima, 1970) or 4 (Akima, 1991) points are collinear. In addition, to ensure the positivity of the interpolating functions, the local algorithm of Fischer et al. (1991) is used, which also preserves the continuity of first order derivatives.

When linear interpolation is adopted, the values of first and second order derivatives at the boundaries are computed using two different methods, depending on the field being derived. As far as diffusivity is concerned, the first order derivative at the boundary is obtained by:

$$\left.\frac{\partial K}{\partial \sigma}\right|_{\mathrm{NLEV}+1} = \frac{K_{\mathrm{NLEV}+1} - K_{\mathrm{NLEV}}}{\sigma_{\mathrm{NLEV}+1} - \sigma_{\mathrm{NLEV}}}, \tag{12}$$

which implies a zero second order derivative. This is assumed because K is expected to be linear near the surface, according to Monin–Obukhov similarity theory where:

$$K(z) = \kappa u_* z, \tag{13}$$

for the neutral case, with proper modifications for diabatic cases. Since, in contrast to K, density is not linear, the requirement is:

$$\left.\frac{\partial^2 \rho}{\partial \sigma^2}\right|_{\mathrm{NLEV}+1} = \left.\frac{\partial^2 \rho}{\partial \sigma^2}\right|_{\mathrm{NLEV}}, \tag{14}$$

GMDD
7, 2797–2828, 2014

which implies:

$$\left.\frac{\partial \rho}{\partial \sigma}\right|_{\mathrm{NLEV}+1} = \left.\frac{\partial \rho}{\partial \sigma}\right|_{\mathrm{NLEV}} + \left.\frac{\partial^2 \rho}{\partial \sigma^2}\right|_{\mathrm{NLEV}} (\sigma_{\mathrm{NLEV}+1} - \sigma_{\mathrm{NLEV}}), \tag{15}$$

for the first order derivative. Following the same considerations made for ρ, the derivatives of σ with respect of z are computed from relationships similar to Eqs. (14) and (15).

Regarding the Akima-spline interpolation, which is implemented only for the K field, a linear profile near the ground is imposed to the interpolating function.

3.3 Integration scheme and time-step selection

The most common integration scheme for SDE in atmospheric transport models is the Euler–Maruyama forward scheme:

$$\Sigma_{t+\Delta t} = \Sigma_t + a\Delta t + b\Delta W. \tag{16}$$

The coefficients a and b come from Eq. (11). The Euler–Maruyama forward scheme is the simplest strong Taylor approximation and turns out to be of order of strong convergence $\gamma = 0.5$ (Kloeden and Platen, 1992, p. 305).

By a rather simple modification of the Euler–Maruyama scheme, i.e. adding the term:

$$\frac{1}{2} b b' (\Delta W^2 - \Delta t), \tag{17}$$

where b' is the first-order derivative of b, the Milstein scheme is obtained, which is of order of strong convergence $\gamma = 1$. It is worth noting that the strong order $\gamma = 1$ of the Milstein scheme corresponds to the strong order $\gamma = 1$ of the Euler deterministic scheme. Therefore, Milstein can be regarded as the correct generalization of the

GMDD
7, 2797–2828, 2014

deterministic Euler scheme (Kloeden and Platen, 1992, p. 345). The additional term uses only already computed quantities (involved in the determination of the drift term of Eq. 11) and therefore its implementation is of negligible computational cost. The Milstein scheme is thus implemented in IL-GLOBO.

In the meteorology component of IL-GLOBO, the Eulerian equations are solved with a macro time-step ΔT, which depends basically on the horizontal resolution due to the limitations imposed by the Courant number. Other time-steps are involved in the Eulerian part but are not relevant here. In typical implementations, ΔT ranges from 432 s for 362×242 point resolution (used for monthly forecasts http://www.isac.cnr.it/dinamica/projects/forecast_dpc/month_en.htm) to 150 s for 1202×818 point resolution (used for high resolution weather forecasts http://www.isac.cnr.it/dinamica/projects/forecasts/glob_newNH/).

The macro time-step is taken as the upper limit for the solution of Eq. (11). The time-step needed to reach the required accuracy depends on the quantities involved in determining the various elements in Eq. (16).

First, a straightforward constraint is that the time-step must satisfy the relationship

$$\sqrt{2K\Delta t_1} \ll K\left(\frac{\partial K}{\partial \sigma}\right)^{-1}, \tag{18}$$

(see, e.g., Wilson and Yee, 2007), which expresses the requirement that the average root-mean square step length must be much smaller than the scale of the variations of K. This gives rise to a limitation that is consistent with the surface layer behavior of the diffusion coefficient, Eq. (13). The condition expressed by Eq. (18) makes Δt_1 vanish for $z \to 0$. Such behavior ensures the WMC to is satisfied theoretically, but clearly poses problems for numerical implementation (Ermak and Nasstrom, 2000; Wilson and Yee, 2007). However, in the application of a global model, where particles can be distributed throughout the troposphere, this problem affects only a small fraction of particles in the vicinity of the surface. Therefore, it can be dealt with by selecting a $\Delta t_{\min}$ small enough

GMDD
7, 2797–2828, 2014

for the solution to be within the accepted error and, at the same time, large enough to not impact on the overall computational cost.

In addition to Eq. (18), another constraint is needed to account also for the presence of a maximum in the K profile, which must be present if one considers the whole atmosphere. At maxima (or minima), Eq. (18) gives an unlimited Δt_1, which is not suitable for the integration of the model as it could cause the trajectory to cross the maximum (or minimum), with a significant change in $K(z)$ associated to a change in $\partial_z K$ sign. To avoid this problem, a further constraint is introduced, based on the normalized second-order derivative, which gives an estimation of the width of the maximum. The constraint reads:

$$2K\Delta t_2 \ll K \left| \frac{\partial^2 K}{\partial \sigma^2} \right|^{-1} . \tag{19}$$

The above Equation has the property of limiting Δt_2 according to the sharpness of the K peak.

Taking the minimum among ΔT, Δt_1 and Δt_2 (and replacing "$\ll$" by "$= C_T$" in Eqs. 18 and 19), gives:

$$\Delta t = \min \left(\Delta T, \frac{C_T}{2} K \left(\frac{\partial K}{\partial \sigma} \right)^{-2}, \frac{C_T}{2} \left| \frac{\partial^2 K}{\partial \sigma^2} \right|^{-1} \right), \tag{20}$$

where the parameter C_T quantifies the "much less" condition and, therefore, must be smaller than at least 0.1. No other arbitrary assumption is needed to define this criterion. Its performance will be evaluated below.

Figure 2 shows the application of Eq. (20) for a K profile representative of GLOBO (see below) and a $C_T = 0.01$. The Δt decreases in the presence of K gradients thanks to condition (18), and is limited around the K maximum (where $\partial K/\partial \sigma = 0$) by condition (19). The maximum of $\Delta t = \Delta T$ is attained at higher levels.

GMDD
7, 2797–2828, 2014

3.4 Boundary conditions

The necessary boundary condition for the conservation of the probability (and therefore of the mass) is the reflective boundary (Gardiner, 1990, p. 121). Wilson and Flesch (1993) show that the elastic reflection ensures the WMC if the integration time-step is small enough. However, in cases of non-homogeneous K, numerical implementation requires that Δt vanishes as the particle approaches the boundary. For models that focus on near surface dispersion, the time-step needed to achieve the required accuracy can become very small. Ermak and Nasstrom (2000) describe a theoretically well founded method to speed-up (roughly by a factor of 10) simulations of this kind.

In the case of IL-GLOBO, it will be shown that the elastic reflection condition at $\sigma = 1$, coupled with the adaptive time step algorithm described in Sect. 3.3, can ensure a good approximation of the solution while maintaining affordable the computational cost.

4 Model verification: the well-mixed condition

In order to test the vertical diffusion module of IL-GLOBO, a series of experiments was performed with a 1-D version of the code. Input profiles were obtained by running the low-resolution version of GLOBO (horizontal grid of 362×242 cells and 50 vertical levels evenly spaced in σ) for the period 11 March 2011–18 March 2011. After 6 h of simulation time, averages on $\sigma = \text{const}$ were performed for K, ρ and z, obtaining vertical profiles as a function of σ. They do not show substantial variation in time and are considered representative of the mean atmosphere. Profiles of ρ and z are rather smooth and regular over space and time, while K displays a large variability. The profiles were fitted with analytical functions for subsequent use. The following analytical expressions were used:

$$\rho(\sigma) = \rho_0 \sigma^{(R_d \Gamma / g + 1)}, \tag{21}$$

GMDD
7, 2797–2828, 2014

and:

$$z(\sigma) = \frac{(\sigma^{-R_d\Gamma/g} - 1)T_0}{\Gamma}, \tag{22}$$

with $T_0 = 288.0\,\mathrm{K}$, $\rho_0 = 1.2\,\mathrm{kg\,m^{-3}}$ and $\Gamma = -0.007\,\mathrm{K\,m^{-1}}$. As can be observed, expressing the density ρ in sigma vertical units ($\rho_\sigma = \rho \left|\frac{\mathrm{d}z}{\mathrm{d}\sigma}\right|$) and using Eqs. (22) and (21), the following constant value is obtained:

$$\rho_\sigma = \frac{\rho_0 R_d T_0}{g}. \tag{23}$$

Figure 3 shows the GLOBO averaged profiles and their fitting functions for the density ρ and the Cartesian coordinate z as function of σ.

As far as the K profile is concerned, the function

$$K(z) = Az \exp\left[-(Bz)^C\right], \tag{24}$$

is used to account for the specific K features: it should display a linear behavior near the surface, must vanish near the boundary layer top[1] and, therefore, must display a maximum at some height. In Eq. (24), $A = 0.23$ was first determined according to average surface-layer properties (the first GLOBO vertical level), and corresponds to a friction velocity $u_* \simeq 0.5$. Then, the other two parameters were let to vary to best fit the average profile giving $B = 3.8 \times 10^{-3}$ and $C = 1.3$.

In the following sections, an alternative K profile is used to test the model in a more critical situation. In fact, the local K profiles resulting from a GLOBO simulation sometimes display isolated strong maxima at the second level above the model surface. This second profile was obtained from Eq. (24) by arbitrarily selecting $B = 2.0 \times 10^{-3}$ and $C = 5.0$. Figure 4 reports the GLOBO averaged, "fitted" and "peaked" K profiles as function of σ.

[1] In GLOBO, K also accounts for a part of the instability generated by moist convection and therefore it may not vanish at the boundary layer top.

GMDD
7, 2797–2828, 2014

4.1 Determination of the optimal setting for the adaptive time-step selection algorithm

The first series of experiments concerns the optimization of the adaptive scheme for Δt, i.e., the selection of the best suited value for the coefficient C_T.

Simulations were performed in flow conditions described by Eqs. (22), (21) and (24), distributing particles with number concentration proportional to ρ. For the WMC to be satisfied, this distribution must remain constant as the time evolves. A number of about 4×10^5 particles were used for all the tests described in this section. Equation (11) was integrated for each particle for 200 macro time-steps, each 432 s long, for a total of $T = 86\,400\,\mathrm{s} = 24\,\mathrm{h}$. Since the initial condition was already well-mixed ($C \propto \rho$), the simulation time was considered sufficient to assess the skill of the model in satisfying the WMC. At the end of the simulation, final profiles were computed of concentration in "σ volume", i.e., $c(\sigma) = N(\sigma)(\Delta\sigma)^{-1}$, where $N(\sigma)$ is the number of particles between σ and $\sigma + \Delta\sigma$. The skill of the model in reproducing the WMC was evaluated using the root mean square error (RMSE) of the final normalized concentration profile with respect to the normalized density profile (derived using Eq. 23).

Simulations were performed using 4 cores of an Intel Xeon machine.

Figure 5 reports the different profiles of concentration after 24 h of simulation computed using different values of C_T. The shaded region represents the interval between 3 standard deviations from the expected value. RMSE values for each simulation are reported in Table 1 along with the computation time. The RMSE error becomes comparable to the statistical error for $C_T = 0.01$, which is selected as the optimal value.

It is also worth noting that the time-step selection algorithm with the proper choice of C_T ensures that the WMC is satisfied at the reflective boundary too, as mentioned in Sect. 3.4.

GMDD
7, 2797–2828, 2014

4.2 Evaluation of the interpolation algorithms

In the subsequent set of experiments, the model skill in reproducing the WMC was evaluated for various resolutions and different interpolation algorithms.

The analytical fields described by Eqs. (21), (22) and (24) were sampled on the grids defined in Table 2. The σ values for grid points in the case of non-regular grid are defined by:

$$\sigma_i^{(1/2)} = \beta\zeta_i + \gamma\zeta_i^3 + \delta\zeta_i^4 \,, \tag{25}$$

where $\sigma_i^{(1/2)}$ is the ith semi-integer level, $\zeta_i = i/(\mathrm{NLEV}+1)$, $\beta = 0.78$, $\gamma = 1.44$ and $\delta = 1.22$. The resulting grid has higher resolution near $\sigma = 1$ and a lower resolution for the levels in the center of the domain, where an accurate description of the fields is expected to be less necessary. Grids with 50 points (A, B) are representative of the actual GLOBO resolution, while grids with 100 points are considered as a resolution attainable for specific experiments. Finer grids are included only for testing purposes.

The two interpolation algorithms were tested for different diffusivity profiles and resolutions. The particle number, initial distribution and simulation time were the same as in the experiment described in Sect. 4.1.

The first experiment concerned the linear interpolation algorithm. Figure 6 shows the results for numerical simulations performed with the "fitted" distribution at the various resolutions. The integration time-step and the diffusion coefficient profiles are shown in the upper panel. The lower panel displays the normalized distribution of the particle after 24 h of simulation along with the expected value.

The experiment with grid A deviates from the WMC both near the ground and in the region above the maximum of diffusivity. The experiment with grid B performs noticeably better at the ground, where the resolution is finer than in grid A. All the other experiments give acceptable results, with the only exception of the grid C experiment, which still displays an accumulation of particles near the ground. It can be observed that the resolution of grid C is coarser than that of grid B near the surface.

GMDD
7, 2797–2828, 2014

Figure 7 shows the same quantities as Fig. 6 for the case of the "peaked" K profile. None of the resolutions produced results that fulfill the WMC. The same also true for the highest resolution (grid F), with a clearly visible depletion of particles in the area of strong gradient above the K maximum. An additional reduction of the integration time-step by a factor of 10^2 did not improve the result (not shown).

The problem could be related to the inconsistency between interpolated functions and their derivatives (first- and second-order) as a result of the linear interpolation between the grid points. The numerical algorithm computes derivatives at the grid points and then linearly interpolates functions and derivatives. With this choice, first- and second-order derivatives are computed at the same order of approximation at the grid points. However, between grid points the consistency of the different components of the stochastic model is not guaranteed. Although it is appropriate for slowly varying and monotone functions like ρ and z, it is unsuitable for K, because it usually displays a more complex profile and affects both the Wiener stochastic term and the drift term.

The use of an interpolation algorithm of higher order is appropriate in this case. The choice of the Akima cubic spline automatically ensures consistency between values and derivatives and the continuity of the first order derivative. With the additional constraint for non-negative values (see Sect. 3.2), the WMC is formally and numerically ensured, along with the physical consistency of the solution.

One drawback of higher-order polynomial interpolation algorithms is the computational cost. To this end, the computational cost of the Akima algorithms was evaluated, comparing its execution time to that of the linear interpolation algorithm.

Table 3 shows the results of this comparison expressed in terms of execution time (in s) and accuracy (RMSE) for resolutions of 50 and 100 grid points, in experiments with the "fitted" diffusivity distribution. The accuracy of experiments with Akima interpolation is comparable with the results obtained using analytical functions (as expected), and their computational cost is only within a factor of 1.2 compared to that of the linear algorithm.

GMDD
7, 2797–2828, 2014

5 Conclusions

The development of a vertical Lagrangian diffusion model is presented. This constitutes the first step in building IL-GLOBO, a Lagrangian particle model integrated in the Eulerian global circulation model GLOBO. Critical details of the implementation have been analyzed and discussed.

The model is developed including the variable density term and the proper coordinate transformation term. The numerical scheme selected to integrate the SDE is the Milstein scheme, which is of order of strong convergence $\gamma = 1$. Therefore, it should be regarded as the natural extension of the deterministic Euler scheme, in contrast to the so-called Euler–Maruyama scheme, which is merely the "transcription" of the deterministic Euler scheme, but not its equivalent.

An adaptive time-step scheme is proposed to ensure the consistency of the model implementation with the WMC requirements. The time-step selection algorithm is limited not only by the condition imposed by the spatial scale of gradients, but also takes into account the scale of the width of maxima and minima of the diffusion coefficient, where the former criterium fails. It is shown that this algorithm ensures that the error is within an acceptable range also at the reflecting boundaries.

Numerical implementations have to deal with the intrinsic discretization imposed by the grid of the Eulerian meteorological model. Two numerical interpolation and derivation schemes are implemented and tested. One is based on linear interpolation and computation of discrete derivatives of order two. The second is based on a modified Akima (1991) interpolation algorithm.

It is found that in the case of the linear scheme strong gradients and isolated maxima in the diffusivity distribution make the results very sensitive to the spatial resolution and the grid distribution. The model error in representing the WM state is also more sensitive to the interpolation and derivation error than to the time discretization error, as long as we consider a number of grid cells typical of a GLOBO simulation and a reasonable setting for the adaptive time-step scheme.

GMDD
7, 2797–2828, 2014

A vertical stretched grid should be used to solve the Eulerian fields in order to reduce the discretization problem near the ground, but the consequent increase in resolution will not ensure the WMC compliance when strong gradients are present.

The second interpolation method (Akima, 1970, 1991; Fischer et al., 1991), while not guaranteeing the continuity of the second order derivative, gives good results at an acceptable computational cost for 1-D applications of the model, suggesting that the consistency between the value of diffusivity and its derivative is one of the determining factors for attaining the WMC. The applicability of this scheme in the full 3-D model still needs to be tested.

The vertical diffusion model is now ready to be implemented within the 3-D global circulation model GLOBO, adding horizontal diffusion and parallelization, and finally verifying the consistency and numerical efficiency of the approach.

Code availability

The numerical code is released under the GNU Public Licence and is available at http://bolchem.isac.cnr.it/source_code.do.

The software is packed as a library using `autoconf`, `automake` and `libtools` which allows for configuration and installation in a variety of systems. The code is developed in a modular way, permitting the easy improvement of physical and numerical schemes.

Acknowledgements. The software used for the production of this article (model development, model run, data analysis, graphics, typesetting) is Free Software. The authors would like to thank the whole free software community, the Free Software Fundation (http://www.fsfs.org) and the Debian Project (http://www.debian.org). Daniele Rossi was partially supported by the CNR and CMCC agreement: “Impatto degli ‘hot spot’ sui cambiamenti climatici a scala regionale”.

GMDD

7, 2797–2828, 2014

References

Akima, H.: A new method of interpolation and smooth curve fitting based on local procedures, J. Assoc. Comput. Mach., 17, 589–602, 1970. 2805, 2815

Akima, H.: A method of univariate interpolation that has the accuracy of a third-degree polynomial, ACM T. Math. Software, 17, 341–366, 1991. 2805, 2814, 2815

Baklanov, A., Schlünzen, K., Suppan, P., Baldasano, J., Brunner, D., Aksoyoglu, S., Carmichael, G., Douros, J., Flemming, J., Forkel, R., Galmarini, S., Gauss, M., Grell, G., Hirtl, M., Joffre, S., Jorba, O., Kaas, E., Kaasik, M., Kallos, G., Kong, X., Korsholm, U., Kurganskiy, A., Kushta, J., Lohmann, U., Mahura, A., Manders-Groot, A., Maurizi, A., Moussiopoulos, N., Rao, S. T., Savage, N., Seigneur, C., Sokhi, R. S., Solazzo, E., Solomos, S., Sørensen, B., Tsegas, G., Vignati, E., Vogel, B., and Zhang, Y.: Online coupled regional meteorology chemistry models in Europe: current status and prospects, Atmos. Chem. Phys., 14, 317–398, doi:10.5194/acp-14-317-2014, 2014. 2800, 2803

Buzzi, A., Fantini, M., Malguzzi, P., and Nerozzi, P.: Validation of a Limited Area Model in cases of Mediterranean cyclogenesis: surface fields and precipitation scores, Meteorol. Atmos. Phys., 53, 137–153, 1994. 2804

Buzzi, A., Davolio, S., D'Isidoro, M., and Malguzzi, P.: The impact of resolution and of 4-D VAR reanalysis on the simulations of heavy precipitation in MAP cases, Meteorol. Z., 13, 91–97, 2004. 2800

Draxler, R. R. and Hess, G. D.: An overview of the HYSPLIT_4 modelling system for trajectories, dispersion, and deposition, Aust. Meteorol. Mag., 47, 295–308, 1998. 2799

Ermak, D. L. and Nasstrom, J. S.: A Lagrangian stochastic diffusion method for inhomogeneous turbulence, Atmos. Environ., 34, 1059–1068, 2000. 2807, 2809

Fiore, A. M., Levy II, H., and Jaffe, D. A.: North American isoprene influence on intercontinental ozone pollution, Atmos. Chem. Phys., 11, 1697–1710, doi:10.5194/acp-11-1697-2011, 2011. 2798

Fischer, B., Opfer, G., and Puri, M. L.: A local algorithm for constructing non-negative cubic splines, J. Approx. Theory, 64, 1–16, 1991. 2805, 2815

Gardiner, C. W.: Handbook of Stochastic Methods for Physics, Chemistry and the Natural Sciences, 2nd Edn., Springer-Verlag, 1990. 2804, 2809

Kloeden, P. E. and Platen, E.: Numerical solution of stochastic differential equations, no. 23, in: Applications of Mathematics, Springer-Verlag, 1992. 2804, 2806, 2807

GMDD
7, 2797–2828, 2014

Lorenz, E. N.: Energy and numerical weather prediction, Tellus, 12, 364–373, 1960. 2804
Malguzzi, P., Buzzi, A., and Drofa, O.: The meteorological global model GLOBO at the ISAC-CNR of Italy assessment of 1.5 yr of experimental use for medium-range weather forecasts, Weather Forecast., 26, 1045–1055, doi:10.1175/WAF-D-11-00027.1, 2011. 2800, 2803, 2804
Mircea, M., D'Isidoro, M., Maurizi, A., Vitali, L., Monforti, F., Zanini, G., and Tampieri, F.: A comprehensive performance evaluation of the air quality model BOLCHEM to reproduce the ozone concentrations over Italy, Atmos. Environ., 42, 1169–1185, 2008. 2800
Phillips, N. A.: A coordinate system having some special advantages for numerical forecasting, J. Meteorol., 14, 184–185, 1957. 2803
Pugh, T. A. M., Cain, M., Methven, J., Wild, O., Arnold, S. R., Real, E., Law, K. S., Emmerson, K. M., Owen, S. M., Pyle, J. A., Hewitt, C. N., and MacKenzie, A. R.: A Lagrangian model of air-mass photochemistry and mixing using a trajectory ensemble: the Cambridge Tropospheric Trajectory model of Chemistry And Transport (CiTTyCAT) version 4.2, Geosci. Model Dev., 5, 193–221, doi:10.5194/gmd-5-193-2012, 2012. 2799
Real, E., Orlandi, E., Law, K. S., Fierli, F., Josset, D., Cairo, F., Schlager, H., Borrmann, S., Kunkel, D., Volk, C. M., McQuaid, J. B., Stewart, D. J., Lee, J., Lewis, A. C., Hopkins, J. R., Ravegnani, F., Ulanovski, A., and Liousse, C.: Cross-hemispheric transport of central African biomass burning pollutants: implications for downwind ozone production, Atmos. Chem. Phys., 10, 3027–3046, doi:10.5194/acp-10-3027-2010, 2010. 2800
Reithmeier, C. and Sausen, R.: ATTILA: atmospheric tracer transport in a Lagrangian model, Tellus B, 54B, 278–299, 2002. 2799
Richardson, L. F.: Atmospheric diffusion shown on a distance-neighbor graph, Proc. R. Soc. Lon. Ser.-A, 110, 709–737, 1926.
Sodemann, H., Schwierz, C., and Wernli, H.: Interannual variability of Greenland winter precipitation sources: Lagrangian moisture diagnostic and North Atlantic Oscillation influence, J. Geophys. Res.-Atmos., 113, D03107, doi:10.1029/2007jd008503, 2008. 2800
Stohl, A., Forster, C., Frank, A., Seibert, P., and Wotawa, G.: Technical note: The Lagrangian particle dispersion model FLEXPART version 6.2, Atmos. Chem. Phys., 5, 2461–2474, doi:10.5194/acp-5-2461-2005, 2005. 2799
Taylor, G. I.: Diffusion by continuous movements, Proc. London Math. Soc., 20, 196–211, 1921. 2801

GMDD
7, 2797–2828, 2014

Thomson, D. J.: Criteria for the selection of stochastic models of particle trajectories in turbulent flows, J. Fluid Mech., 180, 529–556, 1987. 2799, 2800, 2801, 2802
Thomson, D. J.: Discussion, Atmos. Environ., 29, p. 1343, 1995. 2799, 2800, 2801, 2802
Venkatram, A.: The parametrization of the vertical dispersion of a scalar in the atmospheric boundary layer, Atmos. Environ., 27A, 1963–1966, 1993. 2801
Wilson, J. D. and Flesch, T. K.: Flow boundaries in random flight dispersion models: enforcing the well-mixed condition, J. Appl. Meteorol., 32, 1695–1707, 1993. 2809
Wilson, J. D. and Yee, E.: A critical examination of the random displacement model of turbulent dispersion, Bound.-Lay. Meteorol., 125, 399–416, 2007. 2807
Wohltmann, I. and Rex, M.: The Lagrangian chemistry and transport model ATLAS: validation of advective transport and mixing, Geosci. Model Dev., 2, 153–173, doi:10.5194/gmd-2-153-2009, 2009. 2799
Yu, H., Chin, M., West, J. J., Atherton, C. S., Bellouin, N., Bergmann, D., Bey, I., Bian, H. S., Diehl, T., Forbert, G., Hess, P., Shulz, M., Shindell, D., Takemura, T., and Tan, Q.: A multi-model assessment of the influence of regional anthropogenic emission reductions on aerosol direct radiative forcing and the role of intercontinental transport, J. Geophys. Res.-Atmos., 118, 700–720, 2013. 2798

GMDD
7, 2797–2828, 2014

Table 1. RMSE and execution time for different C_T.

C_T	RMSE	Time [s]
0.5	0.044	76
0.1	0.037	238
0.01	0.021	1172
0.001	0.021	7317

GMDD
7, 2797–2828, 2014

Table 2. Resolution and grid spacing type for experiments performed in this work.

Grid label	Resolution (#points)	Grid spacing
A	50	regular
B	50	non-regular
C	100	regular
D	100	non-regular
E	200	regular
F	500	regular

GMDD
7, 2797–2828, 2014

Table 3. Execution time and RMSE for experiments made with the flat diffusivity distribution, varying resolution and interpolation method.

Interpolation algorithm	n. points	exec. time	RMSE
Akima-70	50	332 s	0.024
Akima-91	50	327 s	0.023
Linear	50	293 s	0.097
Akima-70	100	582 s	0.022
Akima-91	100	578 s	0.022
Linear	100	497 s	0.059

GMDD
7, 2797–2828, 2014

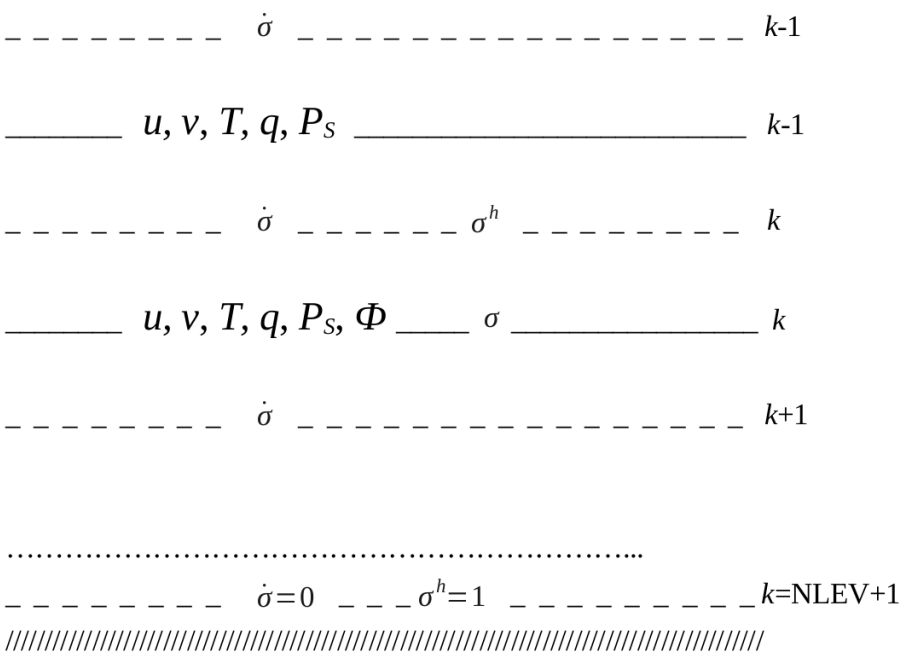

Fig. 1. Schematic representation of field value distributions between integer (continuous lines) and semi integer (dashed lines) levels in the GLOBO model.

GMDD
7, 2797–2828, 2014

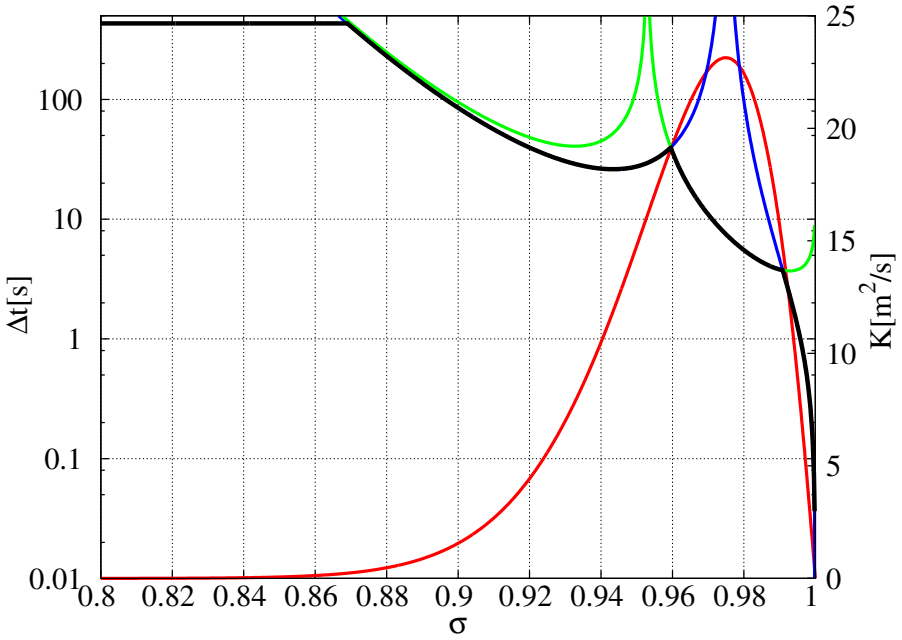

Fig. 2. Values of integration time-step Δt for the diffusivity profile shown by the red curve. The green line shows the contribution of Eq. (18), the blue line the contribution of Eq. (19), and the black line the combined condition (Eq. 20, with $\Delta T = 432\,\mathrm{s}$ and $C_T = 0.01$).

GMDD
7, 2797–2828, 2014

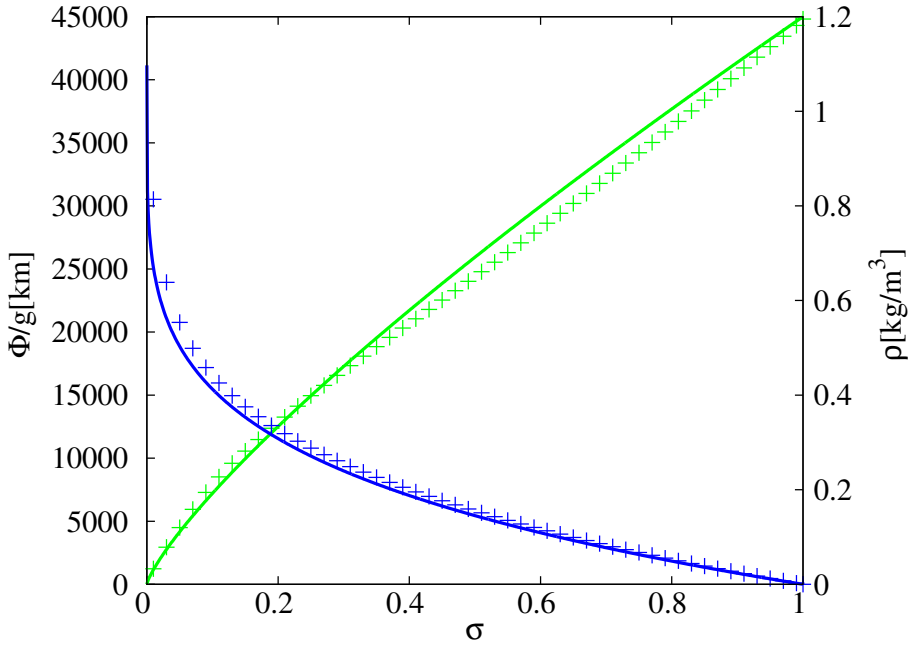

Fig. 3. Average GLOBO profiles of ρ (green symbols) and ϕ/g (blue symbols) as a function of vertical coordinate σ, and their analytical fits (Eqs. 21 and 22, lines of the same colors).

GMDD
7, 2797–2828, 2014

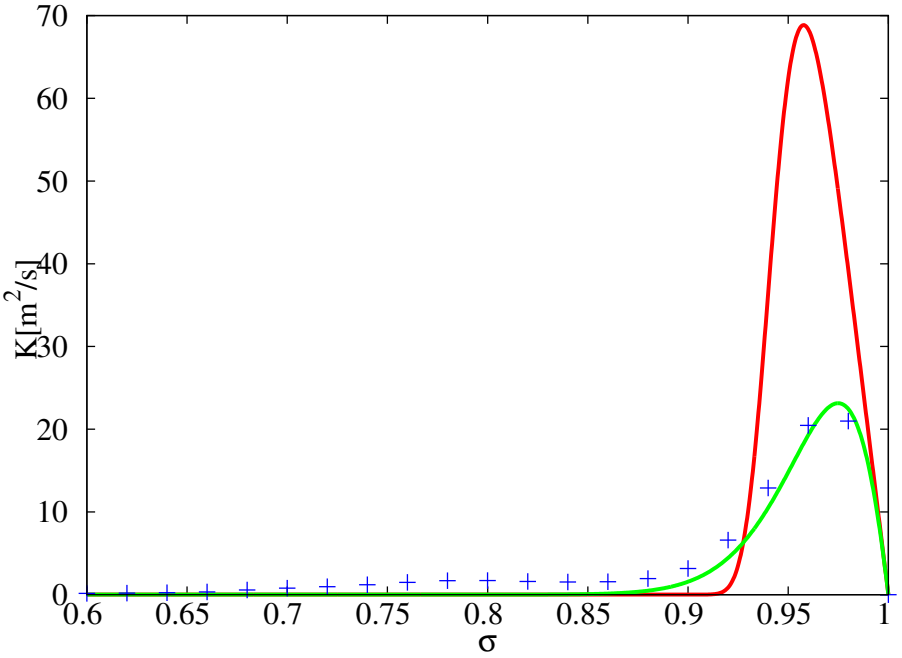

Fig. 4. Diffusivity profiles used in the experiments. The blue symbols show the average K profile from GLOBO. The green curve represents the "fitted" profile, while the red curve represents the "peaked" profile. The functional form of both profiles is described by Eq. (24).

GMDD
7, 2797–2828, 2014

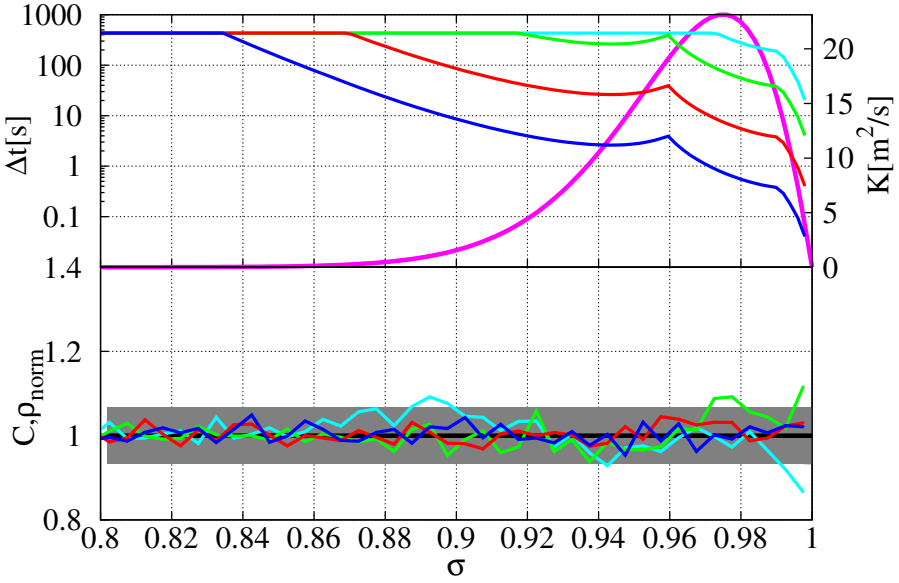

Fig. 5. Dispersion experiment with different choices of parameter C_T. Top panel: diffusivity profile (purple line) and Δt profiles for $C_T = 0.5$ (light blue), $C_T = 0.1$ (green), $C_T = 0.01$ (red) and $C_T = 0.001$ (blue). Bottom panel: normalized concentration profiles for different C_T (line colors as in the top panel).

GMDD
7, 2797–2828, 2014

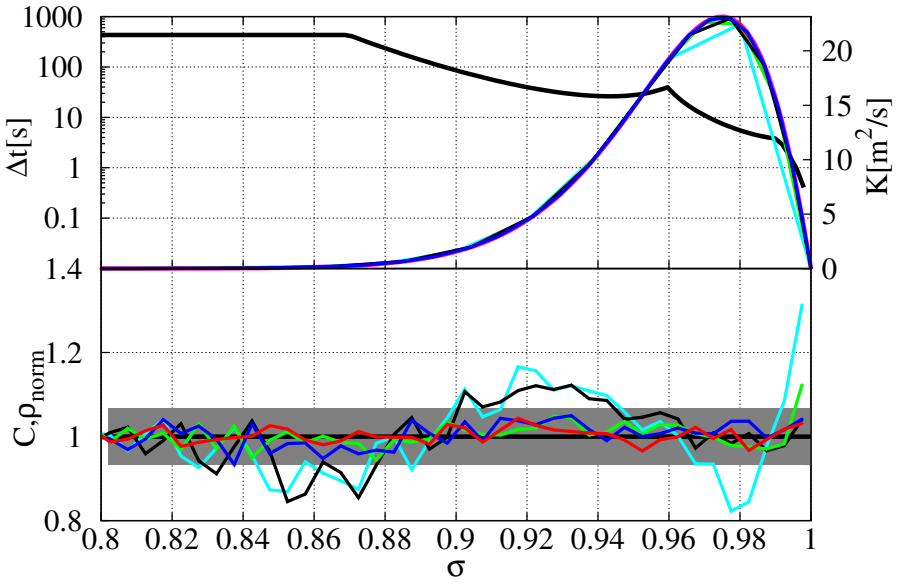

Fig. 6. Test for the linear interpolation algorithm using the "fitted" diffusivity distribution sampled on grids defined in Table 2. Different colors correspond to different grid types: A (light blue), B (black), C (green), D (blue), E (red). Top panel: original (purple continuous line) and sampled diffusivity profile and reference Δt profile (black line). Bottom panel: normalized final concentration (same colors as in the top panel).

GMDD
7, 2797–2828, 2014

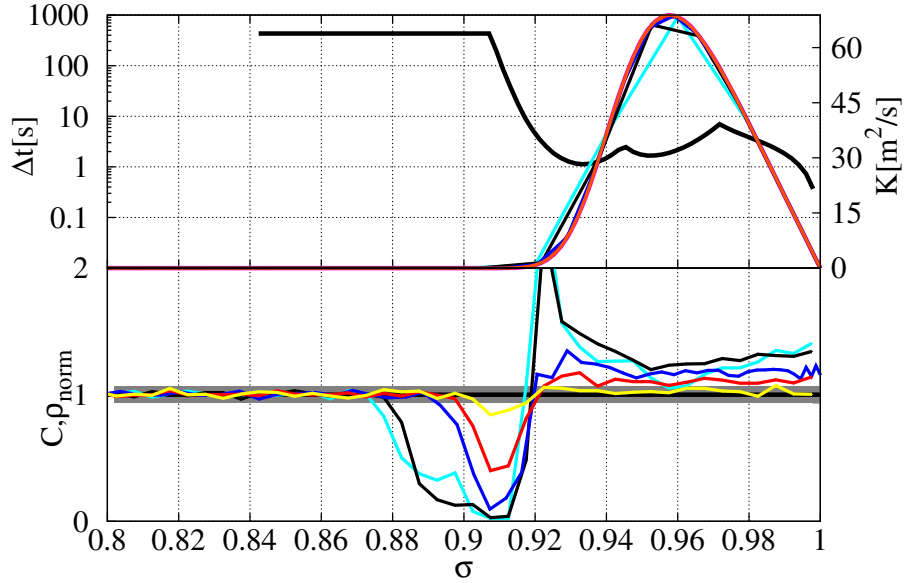

Fig. 7. Same as in Fig. 6 for experiments with the "peaked" diffusivity distribution. Results using grid type F are shown in yellow.

GMDD
7, 2797–2828, 2014